Journal of the Optical Society of America B
OPTICAL PHYSICS

Magneto-optical coaxial waveguide with toroidal magnetization

Nikolay A. Gusev,[1,2,*] Andrey N. Kalish,[1,3] Anatoly K. Zvezdin,[1,2] and Vladimir I. Belotelov[1,3]

[1]Russian Quantum Center, Novaya St. 100, 143025 Skolkovo, Moscow Region, Russia
[2]Prokhorov General Physics Institute, Russian Academy of Sciences, Vavilov St. 38, 119991 Moscow, Russia
[3]Lomonosov Moscow State University, Faculty of Physics, Leninskie Gori, 119991 Moscow, Russia
*Corresponding author: nagusew@gmail.com

Received 22 December 2015; revised 19 April 2016; accepted 7 July 2016; posted 8 July 2016 (Doc. ID 256280); published 27 July 2016

Plasmonic and guided modes of a waveguide constituted by metal walls and a magnetic dielectric core are investigated to reveal how their dispersion and optical field distribution are influenced by a toroidal (azimuthal) magnetization of the core. A phenomenon of the magneto-optical nonreciprocity both in wavenumber and in attenuation coefficient is identified and investigated. It is shown that in the coaxial golden waveguide with the iron-garnet core the nonreciprocity effect reaches maximal values for the plasmonic modes at frequencies above 3×10^{15} rad/s. The effect is of opposite sign for the two types of the plasmonic modes and its value can be tuned by adjusting the geometrical parameters.

OCIS codes: (230.3810) Magneto-optic systems; (230.7370) Waveguides; (240.6680) Surface plasmons.

http://dx.doi.org/10.1364/JOSAB.33.001789

1. INTRODUCTION

Recently, structures with magneto-optical nonreciprocity have become of interest for fundamental and applied research, since they can be used in integrated optics components such as circulators, optical isolators, etc. [1,2]. In magnetoplasmonic structures the nonreciprocity is accompanied by a magnetization-induced shift of the dispersion curves and eigenfrequencies. In particular, in a magnetoplasmonic crystal such a phenomenon leads to a pronounced increase of the transverse magneto-optical Kerr effect [3–6]. Investigation of magnetic and magneto-optical properties of the cylindrical microstructures and nanostructures is partly motivated by their possible application for the novel magnetic field sensors [7]. In that case, magneto-optical effects in such structures can be used for the optical signal reading from a sensitive element.

The dispersion in cylindrical metallic [8] or dielectric [9] waveguides is a well-known problem of radiophysics and optics. The case of a coaxial waveguide of a perfectly conducting metal is described in various literature on radiophysics (see, e.g., [10]). While the authors of [11] studied the coaxial waveguide with protrusions and tranches, the case of a fully dielectric multilayer coaxial waveguide was considered in [12]. Cylindrical and coaxial configurations were compared and the role of plasmons was discussed in [13]. In [14] different configurations of a cylindrical waveguide magnetized along the axis were considered. Reference [15] was devoted to the coaxial waveguide, magnetized along its axis.

Azimuthally magnetized cylindrical and coaxial waveguides are well known and frequently discussed in radiophysics as well [16–19]. One should note the series of papers by Ivanov and Georgiev [18,20,21] and Georgieva-Grosse [22–25] proposing a wave equation for the electric field of TE_{0n} mode and its representation in the form of the confluent hypergeometric function.

In all the aforementioned papers devoted to the problem of wave propagation in azimuthally magnetized cylindrical waveguides, the approximation of an ideal metal was used, and the megahertz frequency range was considered. Such radiophysical formulation excludes finite conductivity of metals and excitation of the surface plasmon polariton (SPP). Recently, in our previous work we have studied circular plasmonic nanorods with toroidal, or azimuthal, magnetization and have found that the emerging magneto-optical nonreciprocity effect is stronger than for the planar case [26].

In the present paper we investigate coaxial and cylindrical waveguides formed by gold walls and toroidally magnetized iron-garnet core. The influence of the magnetization on the waveguide modes and the SPPs at the visible and near-infrared frequency ranges and the properties of the magneto-optical nonreciprocity effect are studied. The core diameter changes from 200 nm to 1 μm. It should be noted that absorption in the metal and dielectric is taken into account. Both analytical and numerical studies are presented.

2. THEORY

Let us consider two golden cylinders; one of them is solid and is placed coaxially inside the other one, which is hollow. The space

between them is filled with a magnetic dielectric of bismuth iron-garnet (BiIG), which is azimuthally magnetized (Fig. 1). Although the total magnetization of the structure equals zero, a nonzero toroidal moment **T** is present [27]. Consequently, the proposed system is a coaxial waveguide with the toroidal magnetic structure. Such a type of magnetic structure can be formed by passing the electric current along the inner metallic cylinder [28]. The current should be strong enough to provide magnetization saturation, so that the magnetization magnitude is constant inside the dielectric. With the z axis of the cylindrical coordinate system directed along the axis of the cylinders, the dielectric permittivity takes the following form:

$$\hat{\epsilon} = \begin{pmatrix} \epsilon_d & 0 & ig \\ 0 & \epsilon_d & 0 \\ -ig & 0 & \epsilon_d \end{pmatrix},$$

where ϵ_d is a permittivity of the nonmagnetized structure, and g is medium gyration, which is proportional to the local magnetization [29]. Each of the field components of the guided modes and the SPPs in the structures of cylindrical symmetry is written as $Z(\rho)\exp[i(kz + l\varphi - \omega t)]$ [8,9,12], where l is the integer valued azimuthal wavenumber; k is the wavenumber along the z axis; ω is the angular frequency; $Z(\rho)$ is a cylindrical amplitude; and ρ, φ, and z are the cylindrical coordinates. In the general case, in the absence of magnetization ($g = 0$) only E_z and H_z field components are independent [9]. In the presence of the toroidal magnetic moment, parallel to the z axis it is not possible to allocate any type of polarization, except the transverse electromagnetic (TEM) one. Consequently, obtaining the wave equation for the individual field components is not possible and an analytical solution cannot be found. However, for the important special case of an axially symmetric field $l = 0$ one can consider two independent types of polarization: TE_{0n} and TM_{0n}. In the first case $\mathbf{E} = \{0, E_\varphi, 0\}$, $\mathbf{H} = \{H_\rho, 0, H_z\}$; and in the second one $\mathbf{E} = \{E_\rho, 0, E_z\}$, $\mathbf{H} = \{0, H_\varphi, 0\}$.

The effect of the toroidal magnetic moment on the TE_{0n} guided modes refers to the radiophysical treatment of the problem, where $\hat{\mu} = \hat{\mu}(g)$ (for the TM_{0n} modes there is no effect on dispersion because $\hat{\epsilon}$ does not depend on magnetization for such a problem), which was considered for the case of an ideal metallic waveguide in [16–25]. In contrast, in this work we investigate ϵ-gyrotropic media and pay attention to the TM_{0n} modes since only for this type of modes the magneto-optical nonreciprocity takes place.

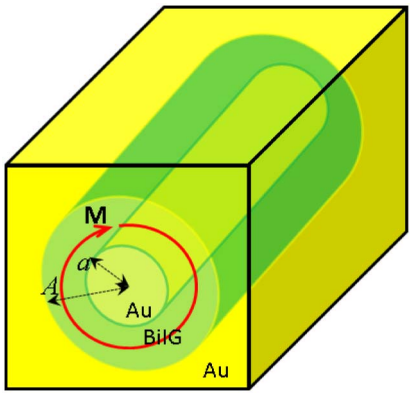

Fig. 1. Structure under consideration. M is magnetization.

From Maxwell's equations the wave equation for the H_φ component of the TM_{0n} mode can be obtained:

$$\rho^2\frac{\partial^2 H_\varphi}{\partial\rho^2} + \rho\frac{\partial H_\varphi}{\partial\rho} + \left(\kappa_d^2\rho^2 + \frac{kg\rho}{\epsilon_d} - 1\right)H_\varphi = 0, \quad (1)$$

for the magnetic dielectric with azimuthal magnetization, and

$$\rho^2\frac{\partial^2 H_\varphi}{\partial\rho^2} + \rho\frac{\partial H_\varphi}{\partial\rho} - (\kappa_m^2\rho^2 + 1)H_\varphi = 0, \quad (2)$$

for the metallic parts of the structure. Here, $\kappa_m^2 = k^2 - k_0^2\epsilon_m$, $\kappa_d^2 = k_0^2\epsilon_d - k^2$, $k_0 = \omega/c$, d indicates BiIG, and m indicates Au; ϵ_m and ϵ_d are the corresponding dielectric constants, and c is the speed of light. In addition, since $g/\epsilon_d \ll 1$ we neglect the quadratic contribution of the magnetization to the propagation constant, i.e., $(\epsilon_d^2 - g^2)/\epsilon_d \approx \epsilon_d$. Equation (2) is a modified Bessel equation with general solution:

$$H_\varphi = C_1 I_1(\kappa_m\rho) + C_2 K_1(\kappa_m\rho), \quad (3)$$

where I_1 and K_1 are modified Bessel functions of the first and second kind, respectively. From the fact that the field must attenuate in the metallic media it is clear that for the internal metal $C_2 = 0$, and for the outer one $C_1 = 0$.

Substituting $H_\varphi = C\rho\exp(-\kappa_d\rho)\zeta(\xi)$, where $\xi = 2\rho\kappa_d$ and C is a constant, one can reduce Eq. (1) to the form

$$\xi\frac{\partial^2\zeta(\xi)}{\partial\xi^2} + (3 - \xi)\frac{\partial\zeta(\xi)}{\partial\xi} - \left(\frac{3}{2} - \frac{g\beta}{2\epsilon_d\kappa_d}\right)\zeta(\xi) = 0. \quad (4)$$

Equation (4) is the Kummer equation. Its general solutions are confluent hypergeometric functions of the first and second kind [30]:

$$\zeta = B_1 M(G, 3, \xi) + B_2 U(G, 3, \xi). \quad (5)$$

Here, $G = 3/2 - gk/2\epsilon_d\kappa_d$.

Finally, magnetic field H_φ of the TM_{0n} mode in a coaxial waveguide in the presence of the toroidal magnetic moment is defined by the following relationship:

$$H_\varphi = B_1 C\rho\exp(-\kappa_d\rho)M(G, 3, 2\kappa_d\rho) + B_2 C\rho\exp(-\kappa_d\rho)U(G, 3, 2\kappa_d\rho). \quad (6)$$

Here, C is a function of ω and k with the dimension of cm^{-1}, which can be found after substituting Eq. (6) into Eq. (1).

Thus, the toroidal magnetic moment affects not only the velocity of propagation of the waveguide mode, but also the optical field distribution, which is generally (at $|gk/2\epsilon_d\kappa_d| \gg 3/2$ or $|gk/2\epsilon_d\kappa_d| \cong 3/2$) not a Bessel type unlike the case of a nonmagnetic waveguide.

For the calculation of the dispersion curves we use the boundary conditions for the field components at the interface. In the case of a conductive metal, the tangential components of the E- and H-fields at the interface between the gold and magnetic dielectric must satisfy the conditions of continuity, which leads to the following relations for the interfaces:

$$\begin{cases} H_{\varphi m} = H_{\varphi d} \\ \frac{1}{\epsilon_m\rho}\frac{\partial(\rho H_{\varphi m})}{\partial\rho} = \frac{1}{\epsilon_d\rho}\frac{\partial(\rho H_{\varphi d})}{\partial\rho} + \frac{gk}{\epsilon_d^2}H_{\varphi d} \end{cases}. \quad (7)$$

Substituting Eq. (6) into Eq. (7) one can obtain the dispersion equation. Since the optical magnetic field in the

waveguide core is expressed as the product of three functions, one of which is a special function, exact analytical solution of the dispersion problem is not straightforward. For simplicity, one can use the fact that usually $|gk/2\epsilon_d\kappa_d| \ll 1$ and, therefore, according to the relationships between confluent hypergeometric functions and Bessel functions [31] at $C = \sqrt{k_0^2\epsilon_d - k^2} = \kappa_d$ Eq. (6) becomes

$$H_\varphi = B_1 J_1(\kappa_d\rho) + B_2 Y_1(\kappa_d\rho), \tag{8}$$

where J_1 and Y_1 are Bessel and Neumann functions, respectively, and Eq. (1) simultaneously switches to a Bessel equation. This simplification means that we neglect the magnetization effect on the distribution of the optical field and in our case the field distribution can be considered as a Bessel one. The correctness of such approximation is confirmed by Fig. 2, where field distribution of Bessel type (H_ϕ at $g = 0$) is compared with the non-Bessel one (H_φ at $g = 0.03$) by the quantity $|\Delta H_\varphi| = |H_\varphi(g = 0) - H_\varphi(g = 0.03)|$. $|\Delta H_\varphi|$ is about 200 times less than Bessel-like H_ϕ. Additionally, as it is seen from the inset in Fig. 2, at $g = 0.03$ (which is a typical value for gyration of BiIG at 600 nm) the distribution of magnetic field $H_\varphi(\rho)$ behaves similarly to Bessel-like $H_\varphi(\rho)$ at $g = 0$. Thus, one can assume that the magnetization only affects the boundary conditions Eq. (7).

Next, substituting Eqs. (8) and (3) into Eq. (7) and taking into account the fact that the field decays as $I_1(\kappa_m\rho)$ inside the inner metallic cylinder and as $K_1(\kappa_m\rho)$ outside the waveguide, we come to the following problem:

$$F(g,k,\omega) = \det(M(g,k,\omega)) = 0;$$

$$M = \begin{pmatrix} I_1(\kappa_m a) & -J_1(\kappa_d a) & -N_1(\kappa_d a) & 0 \\ \frac{\kappa_m}{\epsilon_m} I_0(\kappa_m a) & D_1 & D_2 & 0 \\ 0 & J_1(\kappa_d A) & N_1(\kappa_d A) & -K_1(\kappa_m A) \\ 0 & D_3 & D_4 & \frac{\kappa_m}{\epsilon_m} K_0(\kappa_m A) \end{pmatrix}. \tag{9}$$

Here, a is the radius of the internal cylinder and A is the exterior radius of the waveguide:

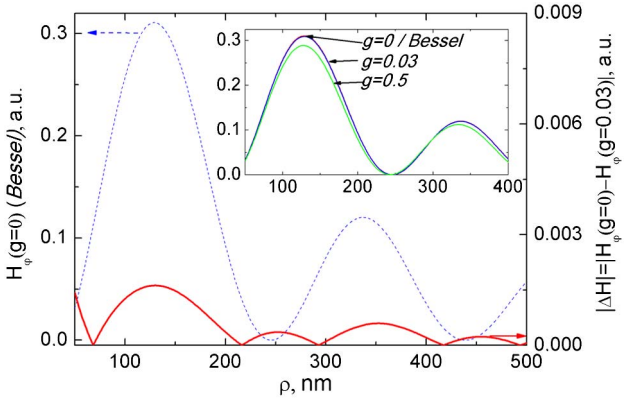

Fig. 2. Influence of the magneto-optical parameter g on the field distribution of $H_\phi(\rho)$ given by Eq. (6). Normalization (coefficients B_1 and B_2) was chosen for reasons of matching Eqs. (6) and (8) at $g = 0$. The result is obtained for $k = 10^5$ cm^{-1}, $\omega = 2.5 \times 10^{15}$ s^{-1}, and $\epsilon_d = 5.34$.

$$\begin{bmatrix} D_1 = -\kappa_d J_0(\kappa_d a)/\epsilon_d - gkJ_1(\kappa_d a)/\epsilon_d^2 \\ D_2 = -\kappa_d Y_0(\kappa_d a)/\epsilon_d - gkY_1(\kappa_d a)/\epsilon_d^2 \\ D_3 = \kappa_d J_0(\kappa_d A)/\epsilon_d + gkJ_1(\kappa_d A)/\epsilon_d^2 \\ D_4 = \kappa_d Y_0(\kappa_d A)/\epsilon_d + gkY_1(\kappa_d A)/\epsilon_d^2. \end{bmatrix}$$

Expanding Eq. (9) the implicit dispersion law can be obtained: $F(\omega, k, g) = 0$, which we do not present here because of its awkwardness. We only note that it is clear already from Eq. (9) that $F(\omega, k, -g) = F(\omega, -k, g) \neq F(\omega, k, g)$, so that the magneto-optical nonreciprocity effect (MONRE) takes place [26].

Additionally, we can obtain the dispersion equation for the eigenmodes in the limit of $a \to 0$, i.e., for a simple cylindrical waveguide with a metal wall. Since in this case one boundary is omitted, for the field on the axis of the waveguide there should be $B_2 = 0$ in Eq. (8), and $C_1 = 0$ in Eq. (3). Using Eq. (7) for the case of a single boundary, we obtain

$$\frac{\kappa_d}{\epsilon_d}\frac{J_0(\kappa_d A)}{J_1(\kappa_d A)} + \frac{\kappa_m}{\epsilon_m}\frac{K_0(\kappa_m A)}{K_1(\kappa_m A)} + \frac{gk}{\epsilon_d^2} = 0. \tag{10}$$

3. RESULTS AND DISCUSSION

A. Dispersion

For numerical calculations the experimental data were used for the real and imaginary parts of gold and BiIG permittivities and for the gyration from [32,33], and both real and imaginary parts of the mode wavenumbers $k = \beta + i\gamma$ were taken into account. Figure 3 shows the dispersion curves $\omega(k)$ for the axisymmetrical modes in the coaxial waveguide for different values of radii a and A in the investigated frequency range of $(1.25 - 3.75) \times 10^{15}$ s^{-1} at **T** oriented along the positive direction of the z axis, which are obtained by numerical solution of Eq. (9). The red dashed line $\omega = c\beta/\sqrt{\epsilon_d}$ indicates a set of (ω, k) values which corresponds to $\kappa_d^2 = 0$ and divides ω-k space into SPP region ($\mathrm{Re}(\kappa_d) = 0$: below the light line, I) and waveguide-mode region ($\mathrm{Re}(\kappa_d) \neq 0$: above the light line, II).

Several types of modes are observed: (i) the "internal SPP" localized at the interface between the inner cylinder and the magnetic filling, (ii) waveguide modes propagating between cylinders, and (iii) the external hybrid waveguide-SPP mode related to the interface between the external metal cylinder and the magnetic filling. The nature of the latter is not pure plasmonic. A similar mode is well known in the theory of planar metal–dielectric–metal structures as the "antisymmetrical mode" (or "low-index mode") [34–36], and the "symmetrical mode" ("high-index mode") corresponds to the "internal SPP." As we can see from the plot, the dispersion curve of the hybrid waveguide-SPP mode is localized partially in the waveguide-mode dispersion region and partially in the SPP region, which is similar for planar metal-dielectric-metal structures [36,37]. With the increase of the outer radius A the number of guided modes grows and the hybrid mode gradually shifts toward the SPP dispersion region. In this case, change in the outer radius A has hardly any effect on the internal SPP, as is seen from Figs. 3(a)–3(c). On the other hand, the change in the inner radius a results in the stronger bending of the dispersion curve of the inner SPP in a coaxial waveguide (Figs. 3(b) and 3(d)), which agrees with our previous studies of nanowires [26].

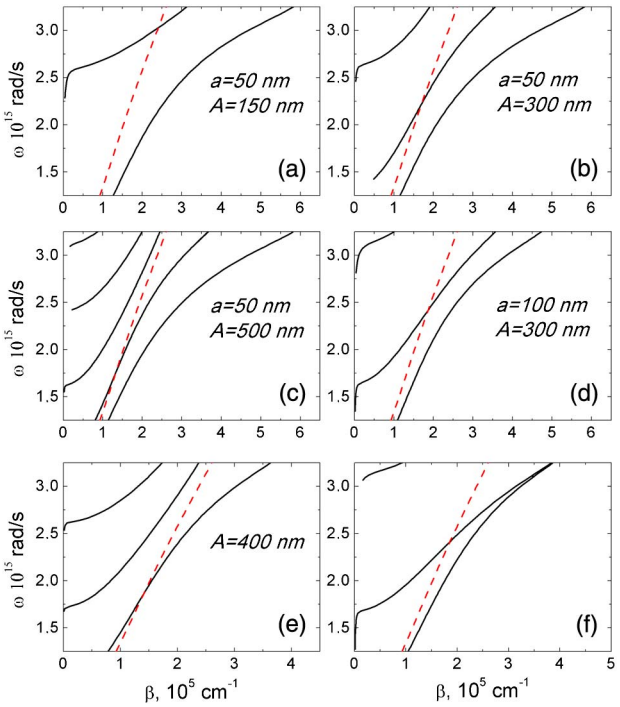

Fig. 3. Mode dispersion for a coaxial waveguide (a)–(d) with different values of size parameters a, A and for cylindrical (e) and planar (f) waveguides. The red dashed line corresponds to $\kappa_d^2 = 0$. The cylindrical waveguide radius is 400 nm and the width of the planar waveguide slab is 200 nm.

However, a small shift of the dispersion curve of the hybrid waveguide-SPP mode toward the SPP dispersion region, caused by the broadening of the gap between the metal surfaces, is observed. Dispersion of the modes in the planar metal–garnet–metal waveguide with the BiIG thickness of 200 nm between the metal surfaces, obtained by solving the corresponding dispersion equation from [38], is shown in Fig. 3(f). Comparison of Figs. 3(d) and 3(f) shows that in the planar case, unlike the coaxial one, the phase velocities of the two SPPs at high frequencies become equal. The difference between the coaxial case from the case of a cylindrical waveguide [Fig. 3(e)], calculated from Eq. (10), lies in the presence of the internal SPP.

The dispersion of higher-order modes ($l \neq 0$) is shown in Fig. 4 with $A = 300$ nm and (a) $a = 50$ nm, or (b) $a = 100$ nm. The analytical solution for the higher-order modes cannot be obtained, so we used a numerical approach based on the finite element method. It can be seen that for each mode with $l = 0$ there are families of corresponding modes with higher l: the SPPs, the waveguide modes, and the hybrid modes. Since each mode in a family behaves similarly to the corresponding axisymmetric mode (basic mode with $l = 0$), within our investigation we mostly focus our attention on the axisymmetric case.

B. Magneto-Optical Nonreciprocity Effect in Cylindrical Waveguides

We now turn to the magneto-optical nonreciprocity effect. It is determined by magnetization-induced variation of the mode

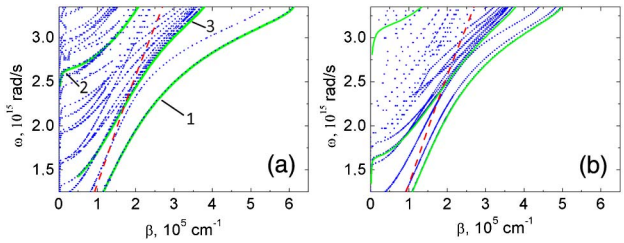

Fig. 4. Dispersion of the modes of different orders ($l = 0, 1, 2\ldots$) for the coaxial waveguide with internal radius (a) $a = 50$ nm and (b) $a = 100$ nm with external radius $A = 300$ nm obtained by FEM modeling (dots). Green solid lines are the corresponding solutions of Eq. (9). Mode 1 is the SPP localized at the interface between the internal cylinder and magnetic filling, modes 2 are the guided modes propagating between metal interfaces, and mode 3 is the guided-SPP mode which behaves like a guided one at lower frequencies, and like an SPP localized at the interface between the external cylinder and the magnetic filling, at higher frequencies.

wavenumber: $\Delta k = k(+g) - k(-g)$, and, consequently, it has real ($\Delta\beta$) and imaginary ($\Delta\gamma$) parts. Figure 5 shows the magnitude of $\Delta\beta(\omega) = \beta(+g, \omega) - \beta(-g, \omega)$ for two configurations: $A = 300$ nm and (a) $a = 50$ nm or (b) $a = 100$ nm. First of all, it should be noted that the MONRE gets largest values for the SPP at the surface of the inner cylinder. The MONRE for the hybrid guided-SPP mode is less but is still larger than for the purely guided modes. The MONREs for the SPP and the guided-SPP are of opposite sign, which is consistent with the fact that the mutual orientation of the mode propagation direction, the magnetization direction, and the arrangement of materials at the interfaces are different. For both cases, the largest value of the magnetization-induced change of $\Delta\beta$ occurs on the bend of the dispersion curves. The effect increases with the frequency.

Blue points correspond to the MONRE of the higher-order modes. As mentioned above, the dispersion of the higher-order modes (SPP, hybrid, and guided modes with $l > 0$) behaves like the dispersion of the corresponding axisymmetric modes with $l = 0$. Wavenumbers of the higher-order modes do not exceed those for the corresponding axisymmetric mode at the same frequency and same **T** (see Fig. 4). Thus, one can

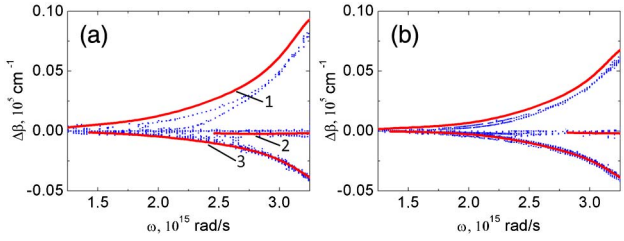

Fig. 5. MONRE in a coaxial waveguide with the radius of the internal cylinder (a) $a = 50$ and (b) $a = 100$ nm for the radius of the external cylinder $A = 300$ nm. Red solid lines indicate the MONRE for axisymmetrical modes obtained by solving Eq. (9) at opposite values of magnetization and blue dots show the values of the effect for the higher-order modes obtained by FEM modeling.

conclude that the MONRE of the higher-order modes behaves like the MONRE of the corresponding axisymmetric mode and does not exceed it (Fig. 5).

Now let us consider the MONRE for different sizes of the waveguide. Figure 6 shows the values of $\Delta\beta(\omega)$ and $\Delta\gamma(\omega) = \gamma(g,\omega) - \gamma(-g,\omega)$ for $a = 50$ nm, $A = 150$, 200, 300, and 500 nm, and for the case of a cylindrical waveguide of radius 150, 200, 300, and 500 nm.

Change of the internal radius a strongly influences the MONRE for the SPP: with decreasing radius the effect increases (see Fig. 5), which is in good agreement with our previous studies of a nanowire [26]. Such phenomenon is explained by a change in the dispersion curves with decreasing radius. The change in the inner radius has no effect on the behavior of the hybrid guided-SPP mode. Similar behavior is observed for the imaginary part of the MONRE $\Delta\gamma$.

The MONRE for the hybrid mode is mainly affected by the change of the external radius A of the coaxial waveguide [Fig. 6(a)]. In this case, the situation is opposite to the case of the pure SPP: with the increase of the outer radius A the effect gets larger. For a cylindrical waveguide the behavior of the MONRE is completely analogous to the case of the hybrid mode in the coaxial waveguide [Figs. 6(b) and 6(d)]. However, for a cylindrical waveguide the effect is larger and varies stronger with the increase of the waveguide radius. At lower frequencies, the MONRE dependence on the radius alters and becomes a decreasing function of the radius.

For pure guided modes the MONRE remains almost unchanged at different radii, compared with the SPP and the hybrid modes, for all cases.

Thus, decreasing the radius of the inner cylinder a, one can increase the MONRE for the SPP, and increasing the exterior radius A, one can increase the MONRE for the hybrid guided-SPP mode. In all cases, the increase of the MONRE is related to changes in phase and group velocities of corresponding modes (see Fig. 3) when the inner radius a and the outer radius A are changed. The MONRE enhancement is due to an increase of the electromagnetic field density in the magnetic environment. The electromagnetic field density of the SPP at the interface between the metal core and the magnetic dielectric grows with decreasing inner radius a, which leads to enhancement of the MONRE for the SPP. At the same time, the MONRE enhancement for the hybrid mode takes place with the growth of the outer radius A that leads to stronger shift of the dispersion curve toward the plasmonic dispersion region [Figs. 3(a) and 3(b)]. It is accompanied by growth of the electromagnetic energy density at the interface between the outer metallic cylinder and magnetic dielectric filling.

The imaginary part of the MONRE [Figs. 6(c) and 6(d)] behaves completely similarly to the real part. The growth is observed only at high frequencies, where there is a strong absorption in gold. At low frequencies, where the absorption is weaker, γ is smaller, and, therefore, $\Delta\gamma$ is smaller as well. The properties of the imaginary part of the MONRE, such

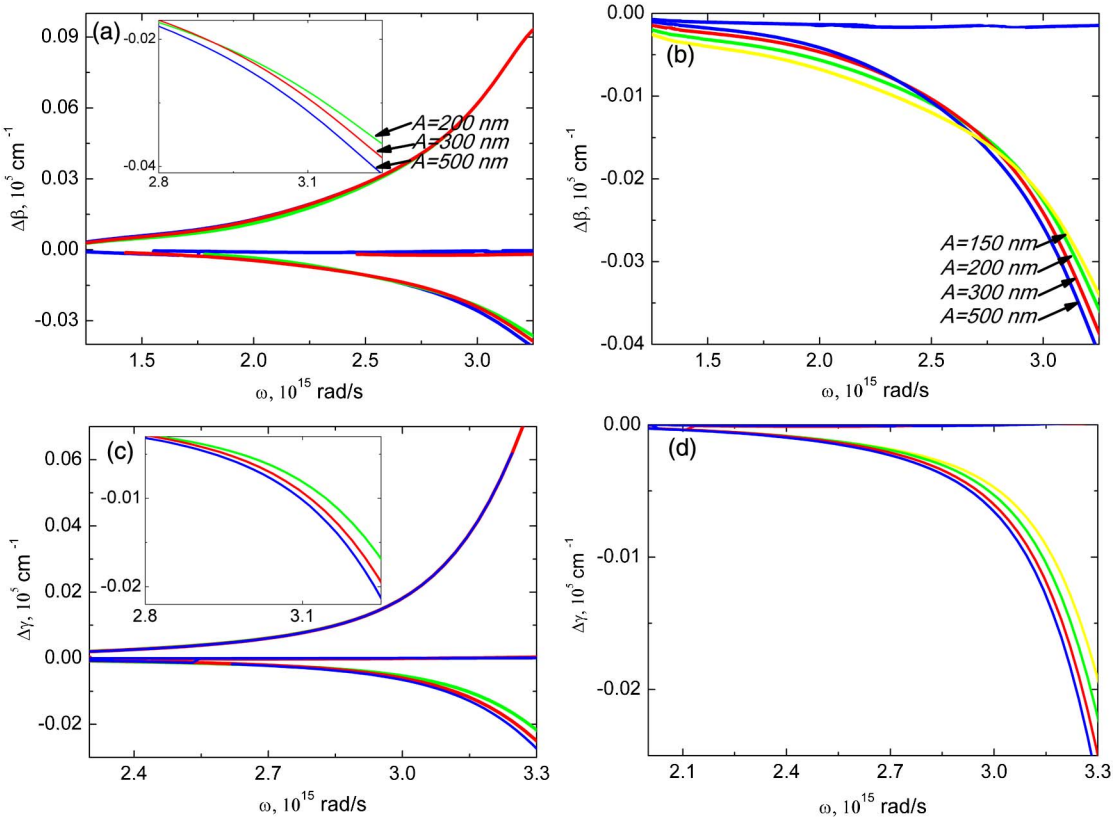

Fig. 6. Real (a), (b) and imaginary (c), (d) parts of the MONRE for axisymmetrical modes in coaxial (a), (c) and cylindrical waveguides (b), (d) with different radii A. The insets show the frequency band segment from 2.8 to 3.25×10^{15} rad/s.

as its dependence on the external radius A, can be explained in the same way as for the real part.

4. CONCLUSION

To conclude, we studied the problem of the azimuthal magnetization impact on the eigenwaves of the coaxial waveguide consisting of metal walls with a magnetic dielectric filling. The investigation was performed for the optical and near-infrared frequency ranges, taking into account the absorption and dichroism. The dispersion equation and expressions for the magnetic field distribution were derived for the eigenmodes with an axisymmetric field of the coaxial and cylindrical waveguides with a toroidal magnetic structure. It was found that this type of magnetization affects the field distribution and the dispersion of eigenmodes. The phenomenon of the magneto-optical nonreciprocity, which is measured by a difference between the phase velocities of the modes propagating in forward and backward directions, was demonstrated. It was found that the MONRE for the SPPs and the waveguide-SPP hybrid modes increases monotonically with frequency. With the increase of the radius of cylinder curvatures (inner radius a or outer radius A of the waveguide) the effect decreases in the former case and increases in the latter one. In all cases, the amplification is associated with the increase of the electromagnetic field concentration in the magnetic dielectric.

Funding. Russian Foundation for Basic Research (RFBR) (14-02-01012, 16-02-01065); Russian Presidential (MD-5763.2015.2).

REFERENCES

1. L. Bi, J. Hu, P. Jiang, D. H. Kim, G. F. Dionne, L. C. Kimerling, and C. A. Ross, "On-chip optical isolation in monolithically integrated non-reciprocal optical resonators," Nat. Photonics **5**, 758–762 (2011).
2. K. Fang, Z. Yu, V. Liu, and S. Fan, "Ultracompact nonreciprocal optical isolator based on guided resonance in a magneto-optical photonic crystal slab," Opt. Lett. **36**, 4254–4256 (2011).
3. L. E. Kreilkamp, V. I. Belotelov, J. Y. Chin, S. Neutzner, D. Dregely, T. Wehlus, I. A. Akimov, M. Bayer, B. Stritzker, and H. Giessen, "Waveguide-plasmon polaritons enhance transverse magneto-optical Kerr effect," Phys. Rev. X **3**, 041019 (2013).
4. M. Pohl, L. E. Kreilkamp, V. I. Belotelov, I. A. Akimov, N. E. Khokhlov, V. J. Yallapragada, A. V. Gopal, M. Nur-E-Alam, M. Vasiliev, D. R. Yakovlev, K. Alameh, A. K. Zvezdin, and M. Bayer, "Tuning of the transverse magneto-optical Kerr effect in magneto-plasmonic crystals," New J. Phys. **15**, 075024 (2013).
5. N. E. Khokhlov, A. R. Prokopov, A. N. Shaposhnikov, V. N. Berzhansky, M. A. Kozhaev, S. N. Andreev, A. P. Ravishankar, V. G. Achanta, D. A. Bykov, A. K. Zvezdin, and V. I. Belotelov, "Photonic crystals with plasmonic patterns: novel type of the heterostructures for enhanced magneto-optical activity," J. Phys. D **48**, 095001 (2015).
6. G. Armelles, A. Cebollada, A. García-Martín, and M. U. González, "Magnetoplasmonics: combining magnetic and plasmonic functionalities," Adv. Opt. Mater. **1**, 10–35 (2013).
7. S. Gudoshnikov, N. Usov, A. Nozdrin, M. Ipatov, A. Zhukov, and V. Zhukova, "Highly sensitive magnetometer based on the off-diagonal GMI effect in Co-rich glass-coated microwire," Phys. Status Solidi **211**, 980–985 (2014).
8. L. Novotny and C. Hafner, "Light propagation in a cylindrical waveguide with a complex, metallic, dielectric function," Phys. Rev. E **50**, 4094–4106 (1994).
9. E. Snitzer, "Cylindrical dielectric waveguide modes," J. Opt. Soc. Am. B **51**, 491–498 (1961).
10. N. Marcuvitz, "Transmission-line modes," in *Waveguide Handbook* (McGraw-Hill, 1951), Chap. 2, p. 72.
11. K. Singh, P. K. Jain, and B. N. Basu, "Analysis of a coaxial waveguide corrugated with wedge-shaped radial vanes considering azimuthal harmonic effects," Prog. Electromagn. Res. **47**, 297–312 (2004).
12. M. Ibanescu, Y. Fink, S. Fan, E. L. Thomas, and J. D. Joannopoulos, "An all-dielectric coaxial waveguide," Science **289**, 415–419 (2000).
13. F. I. Baida, A. Belkhir, D. Van Labeke, and O. Lamrous, "Subwavelength metallic coaxial waveguides in the optical range: role of the plasmonic modes," Phys. Rev. B **74**, 205419 (2006).
14. E. Cojocaru, "Modes in dielectric or ferrite gyrotropic slab and circular waveguides, longitudinally magnetized, with open and completely or partially filled wall," J. Opt. Soc. Am. B **27**, 1965–1977 (2010).
15. M. Yang, L. T. Wu, T. J. Guo, R. P. Guo, H. X. Cui, X. W. Cao, and J. Chen, "Study on photonic angular momentum states in coaxial magneto-optical waveguides," J. Appl. Phys. **116**, 153104 (2014).
16. R. S. Mueller and F. J. Rosenbaum, "Propagation along azimuthally magnetized ferrite-loaded circular waveguides," J. Appl. Phys. **48**, 2601–2603 (1977).
17. A. E. Mudrov, V. A. Meshcheryakov, and G. A. Red'Kin, "Coaxial waveguide with azimuthally magnetized gyrotropic filling," Russ. Phys. J. **22**, 552–554 (1979).
18. K. P. Ivanov and G. N. Georgiev, "Some properties of the circular waveguide with azimuthally magnetized ferrite," J. Appl. Phys. **67**, 6529–6537 (1990).
19. N. Dib and A. Omar, "Dispersion analysis of multilayer cylindrical transmission lines containing magnetized ferrite substrates," IEEE Trans. Microwave Theory Tech. **50**, 1730–1736 (2002).
20. K. P. Ivanov and G. N. Georgiev, "Asymptotic study of rotationally symmetric waves in a circular anisotropic waveguide," in *IEE Proceedings H—Microwaves, Antennas and Propagation* (IET Digital Library, 1985), Vol. **132**, pp. 261–266.
21. K. P. Ivanov and G. N. Georgiev, "On a class of electromagnetic wave functions for propagation along the circular gyrotropic waveguide," IEEE Trans. Microwave Theory Tech. **34**, 853–862 (1986).
22. G. N. Georgiev and M. N. Georgieva-Grosse, "The Kummer confluent hypergeometric function and some of its applications in the theory of azimuthally magnetized circular ferrite waveguides," J. Telecommun. Inf. Technol. **3**, 112–128 (2005).
23. G. N. Georgiev and M. N. Georgieva-Grosse, "Iterative method for differential phase shift computation in the azimuthally magnetized circular ferrite waveguide," Prog. Electromagn. Res. **6**, 365–369 (2010).
24. G. N. Georgiev and M. N. Georgieva-Grosse, "Analysis of the differential phase shift in the circular ferrite-dielectric waveguide with azimuthal magnetization," in *Antennas and Propagation Society International Symposium (APSURSI)* (IEEE, 2010), pp. 1–4.
25. G. N. Georgiev and M. N. Georgieva-Grosse, "Advanced computational methods for analysis of the circular waveguide completely filled with azimuthally magnetized ferrite: review of recent results," in *International Conference on Electromagnetics in Advanced Applications (ICEAA)* (IEEE, 2012), pp. 62–65.
26. N. A. Gusev, V. I. Belotelov, and A. K. Zvezdin, "Surface plasmons in nanowires with toroidal magnetic structure," Opt. Lett. **39**, 4108–4111 (2014).
27. A. N. Kalish, V. I. Belotelov, and A. K. Zvezdin, "Optical properties of toroidal media," Proc. SPIE **6728**, 67283D (2007).
28. M. Ipatov, V. Zhukova, A. Zhukov, J. Gonzalez, and A. Zvezdin, "Low-field hysteresis in the magnetoimpedance of amorphous microwires," Phys. Rev. B **81**, 134421 (2010).
29. A. K. Zvezdin and V. A. Kotov, *Modern Magnetooptics and Magnetooptical Materials* (JM Arrowsmith, 1997).
30. A. Cuyt, V. B. Petersen, B. Verdonk, H. Waadeland, and W. B. Jones, "Confluent hypergeometric functions," in *Handbook of Continued Fractions for Special Functions* (Springer, 2008), Chap. 16, p. 320.
31. N. N. Lebedev, "Hypergeometric functions," in *Special Functions and Their Applications* (Prentice-Hall, 1965), Chap. 9, p. 274.
32. E. D. Palik, *Handbook of Optical Constants of Solids* (Academic, 1985).

33. M. Vasiliev, P. C. Wo, K. Alameh, P. Munroe, Z. Xie, V. A. Kotov, and V. I. Burkov, "Microstructural characterization of sputtered garnet materials and all-garnet magnetic heterostructures: establishing the technology for magnetic photonic crystal fabrication," J. Phys. D **42**, 135003 (2009).
34. B. Prade, J. Y. Vinet, and A. Mysyrowicz, "Guided optical waves in planar heterostructures with negative dielectric constant," Phys. Rev. B **44**, 13556–13572 (1991).
35. D. Nikolova and A. J. Fisher, "Switching and propagation of magnetoplasmon polaritons in magnetic slot waveguides and cavities," Phys. Rev. B **88**, 125136 (2013).
36. P. Ginzburg, D. Arbel, and M. Orenstein, "Gap plasmon polariton structure for very efficient microscale-to-nanoscale interfacing," Opt. Lett. **31**, 3288–3290 (2006).
37. R. L. Chern, C. C. Chang, and C. C. Chang, "Analysis of surface plasmon modes and band structures for plasmonic crystals in one and two dimensions," Phys. Rev. E **73**, 036605 (2006).
38. V. I. Belotelov, I. A. Akimov, M. Pohl, A. N. Kalish, S. Kasture, A. S. Vengurlekar, A. V. Gopal, V. A. Kotov, D. Yakovlev, A. K. Zvezdin, and M. Bayer, "Intensity magnetooptical effect in magnetoplasmonic crystals," J. Phys. **303**, 012038 (2011).